Titre: Title:	Time-reversal routing for dispersion code multiple access (DCMA) communications
Auteurs: Authors:	Lianfeng Zou, & Christophe Caloz
Date:	2018
Type:	Article de revue / Article
Référence: Citation:	Zou, L., & Caloz, C. (2018). Time-reversal routing for dispersion code multiple access (DCMA) communications. IEEE Access, 6, 9650-9654. https://doi.org/10.1109/access.2018.2805869

Titre de la revue: Journal Title:	IEEE Access (vol. 6)
Maison d'édition: Publisher:	IEEE
URL officiel: Official URL:	https://doi.org/10.1109/access.2018.2805869
Mention légale: Legal notice:	

Received January 12, 2018, accepted February 7, 2018, date of publication February 15, 2018, date of current version March 13, 2018.

Digital Object Identifier 10.1109/ACCESS.2018.2805869

Time-Reversal Routing for Dispersion Code Multiple Access (DCMA) Communications

LIANFENG ZOU, (Student Member, IEEE), AND CHRISTOPHE CALOZ, (Fellow, IEEE)
Electrical Engineering Department, École Polytechnique de Montréal, Montréal, QC H3T 1J4, Canada

Corresponding author: Lianfeng Zou (lianfengzou@gmail.com)

ABSTRACT We present the modeling and characterization of a time-reversal routing dispersion code multiple access (TR-DCMA) system. We show that this system maintains the low complexity advantage of DCMA transceivers while offering dynamic adaptivity for practical communication scenarios. We first derive the mathematical model and explain operation principles of the system, and then characterize its interference, signal to interference ratio and bit error probability characteristics.

INDEX TERMS Dispersion engineering, phaser, time-reversal (TR), dispersion code multiple access (DCMA), routing.

I. INTRODUCTION

Real-time Analog Signal Processing (R-ASP) is a new paradigm for future millimeter-wave and terahertz high-speed wireless communications [1]. It consists in processing high-frequency ultrawide-band RF signals in *real time* using dispersion-engineering electromagnetic components called "phasers," which are analog processor providing application-specific group delay responses [1], [2]. R-ASP applications reported to date include spectrum analysis [3], spectrum sniffing [4], time-stretching based sampling enhancement [5]–[7], time reversal [8], chipless RFID [9], communication SNR enhancement [10] and dispersion code multiple access (DCMA) wireless communication [11], [12]. Given its real-time nature, R-ASP technology is particularly promising for 5G, where high capacity, low latency and small consumption are essential requirements [13].

R-ASP DCMA is a novel wireless access point technology, introduced [12], where each access point is assigned a distinct dispersion code, or a specified group delay function, provided by a phaser, characterized by low transceiver complexity, in addition to the aforementioned advantages of high-capacity, low latency and small consumption inherent to R-ASP [12]. However, the DCMA system [12] can only route signals between *fixed* communication pairs. For *dynamic* routing between arbitrary pairs, an adaptivity strategy must be introduced. One solution may be to use active phasers that reconfigure in real time to match the group delay profiles between arbitrary access point pairs [14], but such phasers are complex and still at an early development stage. For this reason, we propose a routing station, or router, where routing is performed using *time reversal*, previously used mainly for acoustic and electromagnetic wave focusing [15], [16].

II. SYSTEM DESCRIPTION

Figure 1 shows a diagrammatic representation of the proposed Time-Reversal Dispersion Code Multiple Access (TR-DCMA) routing system with $2M$ access points (AP) and the router with endowed with time reversal capability. Uplink $\mathrm{AP}_m^{\mathrm{U}}$, $m \in \{1, \ldots, M\}$, communicates with downlink $\mathrm{AP}_{n(m)}^{\mathrm{D}}$, $n(m) \in \{1, \ldots, M\}$, via the router, where $n(m)$ is a function of m corresponding to the desired routing link from access point m to access point n, with $n(m_1) \neq n(m_2)$ for $m_1 \neq m_2$.

For multiple access purpose, $\mathrm{AP}_k^{\mathrm{U/D}}$ is assigned a specific dispersion code, which is the group delay function $\tau_k^{\mathrm{U/D}}(\omega)$, provided by the coding phaser [1] that is incorporated in the AP system before/after the antenna. The phaser impulse response $g_k^{\mathrm{U/D}}(t)$ is found by inverse Fourier transforming ($\mathcal{F}^{-1}$) the transfer function $G_k^{\mathrm{U/D}}(\omega)$ as

$$g_k^{\mathrm{U/D}}(t)=\mathcal{F}^{-1}\left[G_k^{\mathrm{U/D}}(\omega)\right]=\mathcal{F}^{-1}\left[\mathrm{rect}\left(\frac{\omega-\omega_0}{\Delta\omega}\right)e^{j\phi_k^{\mathrm{U/D}}(\omega)}\right], \tag{1a}$$

where

$$\phi_k^{\mathrm{U/D}}(\omega) = -\int_{\omega_0-\Delta\omega/2}^{\omega} \tau_k^{\mathrm{U/D}}(\omega')\,d\omega', \tag{1b}$$

and $\tau_k^{\mathrm{U/D}}(\omega)$ are the phaser transfer phase and group delay (dispersion code), respectively, and $\omega_0 = 2\pi f_0$, $\Delta\omega = 2\pi\Delta f$ are the center frequency and bandwidth, respectively. The *wireless* channel between the AP (after/before the phaser) and

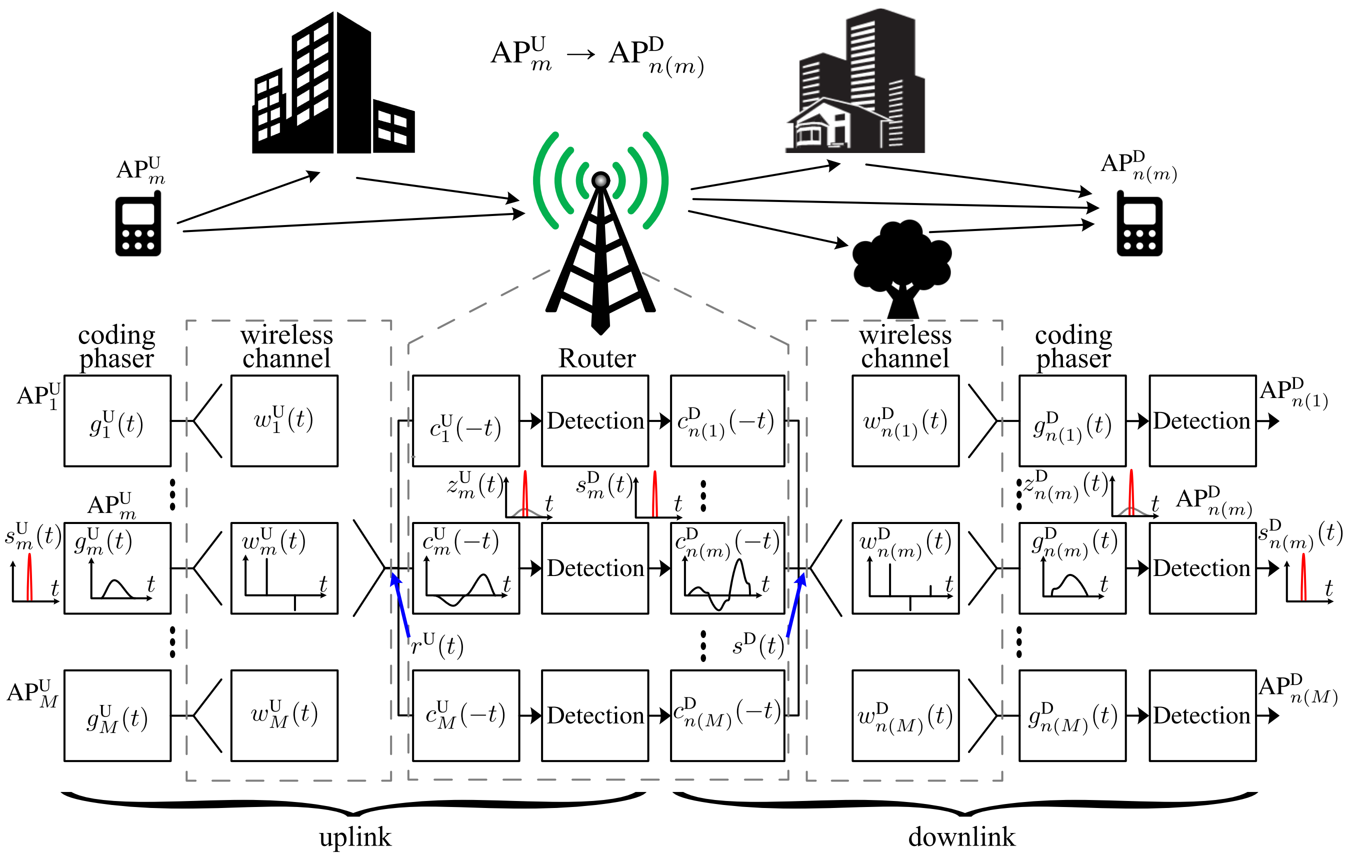

FIGURE 1. **Diagrammatic representation of the proposed TR-DCMA system.**

the router, denoted as $w_k^{\mathrm{U/D}}(t)$, naturally includes the AP and the router antenna impulse responses in the communication direction and typically exhibits multipath fading [17].

III. MODELING

A. CALIBRATION PHASE

During this phase, the $2M$ APs sequentially send a known beacon signal, $s^{\mathrm{B}}(t)$, to the router. The router receives for $\mathrm{AP}_k^{\mathrm{U/D}}$ the signal

$$\begin{aligned} r_k^{\mathrm{B,U/D}}(t) &= \left[(s^{\mathrm{B}} * g_k^{\mathrm{U/D}}) * w_k^{\mathrm{U/D}}\right](t) \\ &= \left(s^{\mathrm{B}} * c_k^{\mathrm{U/D}}\right)(t), \end{aligned} \tag{2a}$$

where

$$c_k^{\mathrm{U/D}}(t) = (g_k^{\mathrm{U/D}} * w_k^{\mathrm{U/D}})(t), \tag{2b}$$

is the overall channel impulse response, corresponding to the convolution ("$*$") of the corresponding *guided-wave* channel (coding phaser) and *wireless* channel impulse response.

Since $s^{\mathrm{B}}(t)$ is known, $c_k^{\mathrm{U/D}}(t)$ can be determined from (2a) by the router. This may be done either digitally or analogically. In the former case, the measured signal $r_k^{\mathrm{U/D}}(t)$ is stored, then numerically deconvolved and flipped, i.e. $c_k^{\mathrm{U/D}}(t) \to c_k^{\mathrm{U/D}}(-t)$, and finally reconverted to the analog domain. In the latter case, which is more advantageous in terms of latency, $r_k^{\mathrm{U/D}}(t)$ is immediately deconvolved by the (known) time-reversed version of $s^{\mathrm{B}}(t)$, $s^{\mathrm{B}}(-t)$, using a real-time convolver [18], yielding $c_k^{\mathrm{U/D}}(t)$, which is itself time-reversed by a real-time time reverser [8] into $c_k^{\mathrm{U/D}}(-t)$.

B. COMMUNICATION PHASE

1) UPLINK TRANSMISSION

Assume the worst-case scenario where the M uplink APs are sending their signals at the same time. Denoting $s_m^{\mathrm{U}}(t)$ the signal sent from $\mathrm{AP}_m^{\mathrm{U}}$, the signal received by the router is

$$r^{\mathrm{U}}(t) = \sum_{m=1}^{M} \alpha_m^{\mathrm{U}} s_m^{\mathrm{U}}(t) * c_m^{\mathrm{U}}(t), \tag{3}$$

where $\alpha_m^{\mathrm{U}} > 0$ is the sent signal magnitude. The decoding of the signal from $\mathrm{AP}_m^{\mathrm{U}}$ at the router consists in convolving $r^{\mathrm{U}}(t)$ with the time-reversed version of the corresponding channel impulse response $c_m^{\mathrm{U}}(-t)$ constructed in the calibration phase [Sec. (III-A)]. Thus,

$$z_m^{\mathrm{U}}(t) = r^{\mathrm{U}}(t) * c_m^{\mathrm{U}}(-t) = \tilde{s}_m^{\mathrm{U}}(t) + x_m^{\mathrm{U}}(t), \tag{4a}$$

where

$$\tilde{s}_m^{\mathrm{U}}(t) = \alpha_m^{\mathrm{U}} s_m^{\mathrm{U}}(t) * c_m^{\mathrm{U}}(t) * c_m^{\mathrm{U}}(-t) \approx \alpha_m^{\mathrm{U}} s_m^{\mathrm{U}}(t), \tag{4b}$$

is an approximation of the desired signal, $s_m^{\mathrm{U}}(t)$, the approximation (rather equality) being due to the finite calibration time in (2b),[1] and

$$x_m^{\mathrm{U}}(t) = c_m^{\mathrm{U}}(-t) * \sum_{\substack{k=1\\k\neq m}}^{M} \alpha_k^{\mathrm{U}} s_k^{\mathrm{U}}(t) * c_k^{\mathrm{U}}(t), \tag{4c}$$

is a distortion signal called multiple-access interference (MAI).

2) ROUTER DETECTION

At this point, the uplink signal $z_m^{\mathrm{U}}(t)$ in (4), including the desired information $\tilde{s}_m^{\mathrm{U}}(t)$ and interference from the other channels $x_m^{\mathrm{U}}(t)$, is passed through a threshold detector in the router (Fig. 1), which transforms it into the signal $s_m^{\mathrm{D}}(t)$.

3) DOWNLINK TRANSMISSION

In the downlink transmission process, the signal $s_m^{\mathrm{D}}(t)$ is to be routed to $\mathrm{AP}_{n(m)}^{\mathrm{D}}$, the desired corresponding access point, that generally varies in time. For this purpose, it is first predistorted by convolution with the time-reversed version of the corresponding downlink channel impulse response, $c_{n(m)}^{\mathrm{D}}(-t)$. Then, the M predistorted signals are combined and sent by the antenna of the router as

$$s^{\mathrm{D}}(t) = \sum_{m=1}^{M} \alpha_m^{\mathrm{D}} s_m^{\mathrm{D}}(t) * c_{n(m)}^{\mathrm{D}}(-t), \ \ \alpha_m^{\mathrm{D}} > 0. \tag{5}$$

After passing the wireless channel $w_{n(m)}^{\mathrm{D}}(t)$, this signal is decoded by phaser $g_{n(m)}^{\mathrm{D}}(t)$ as

$$\begin{aligned} z_{n(m)}^{\mathrm{D}}(t) &= s^{\mathrm{D}}(t) * w_{n(m)}^{\mathrm{D}}(t) * g_{n(m)}^{\mathrm{D}}(t) \\ &= s^{\mathrm{D}}(t) * c_{n(m)}^{\mathrm{D}}(t) \\ &= \tilde{s}_{n(m)}^{\mathrm{D}}(t) + x_{n(m)}^{\mathrm{D}}(t), \end{aligned} \tag{6a}$$

where

$$\tilde{s}_{n(m)}^{\mathrm{D}}(t) = \alpha_m^{\mathrm{D}} s_m^{\mathrm{D}}(t) * c_{n(m)}^{\mathrm{D}}(-t) * c_{n(m)}^{\mathrm{D}}(t) \approx \alpha_m^{\mathrm{D}} s_m^{\mathrm{D}}(t) \tag{6b}$$

and

$$x_{n(m)}^{\mathrm{D}}(t) = c_{n(m)}^{\mathrm{D}}(t) * \sum_{\substack{k=1\\k\neq m}}^{M} \alpha_k^{\mathrm{D}} s_k^{\mathrm{D}}(t) * c_{n(k)}^{\mathrm{D}}(-t). \tag{6c}$$

The following threshold detection (Fig. 1) yields $s_{n(m)}^{\mathrm{D}}(t)$. Communication is naturally successful when the detected downlink signal is identical to the transmitted uplink signal, i.e. $s_{n(m)}^{\mathrm{D}}(t) = s_m^{\mathrm{D}}(t) = s_m^{\mathrm{U}}(t)$.

In addition to the benefits inherent to R-ASP, the proposed time-reversal routing scheme offers the following advantage when performed analogically, as discussed in Sec. III-A. In this case, it is naturally performed at the *physical layer* of the base station. This eliminates the *routing latency* produced by the transfer to the *protocol layer* in conventional routing schemes (e.g. Evolved Packet Core in LTE [19]) [13], [19].

[1] If the calibration time were infinite, then we would have an equality from the identity $c_m^{\mathrm{U}}(t) * c_m^{\mathrm{U}}(-t) = \delta(t)$. In practice, $c_m^{\mathrm{U}}(t)$ in (4b) is a *truncated* version of the ideal $c_m^{\mathrm{U}}(t)$ function.

IV. SYSTEM CHARACTERIZATION

This section characterizes the proposed time-reversal routing DCMA system in terms of MAI, signal to interference ratio (SIR) and bit error probability (BEP) for the case of On-Off Keying (OOK) modulation and Chebyshev dispersion coding. Note that, since uplink and downlink signals are described by mathematical expressions, Eqs. (4) and (6), of the same form, we shall consider here only the uplink case, the downlink and overall transmission being immediately deducible from it.

A. MODULATION AND CODING

Assuming OOK modulation, the transmitted signal is the pulse train

$$s_m^{\mathrm{U}}(t) = \sum_{\ell} d_{m\ell}^{\mathrm{U}} \delta(t - \ell T_{\mathrm{b}} - t_m^{\mathrm{U}}), \tag{7}$$

where $d_{m\ell}^{\mathrm{U}} = 1$ or 0 is the ℓ^{th} base-band bit, $\delta(\cdot)$ is the Dirac function, T_{b} is bit period and t_m^{U} is a random time offset.

Following [12], we choose odd Chebyshev dispersion coding $[\tau_m^{\mathrm{U}}(\omega)]$ for $\mathrm{AP}_m^{\mathrm{U}}$, $\forall\, m$, corresponding to

$$\tau_m^{\mathrm{U}}(\omega) = \tau_0 + \frac{\Delta\tau}{2} T_{i(m)} \left(\frac{\omega - \omega_0}{\Delta\omega/2} \right), \tag{8}$$

where $\Delta\tau$ is group delay swing over the band $\Delta\omega$, $T_{i(m)}$ is $i(m)^{\mathrm{th}}$ order Chebyshev polynomial of the first kind, and where we define $T_{-i(m)} = -T_{i(m)}$ for $i(m) > 0$. The code set of the M uplink access points may then be written

$$\mathbf{C} = \{i(1), \ldots, i(m), \ldots, i(M)\}, \ \ i(m) \text{ odd and } i(m) \geq 3. \tag{9}$$

In the forthcoming computations, we consider the CM3 type (4–10 m NLOS) indoor multipath channel [20] for $w_m^{\mathrm{U}}(t)$.

B. MAI PROBABILITY DENSITY FUNCTION

In [12], we have shown that in a LOS wireless channel, the MAI corresponding to all-odd Chebyshev dispersion coding (9) follows a normal distribution. We shall show here that the same is true for non-LOS.

Figure 2 plots uplink simulation results of an $M = 5$ TR-DCMA system for three different bit periods (T_{b}) in the worst-case interference scenario where all the transmitters continuously send the bit '1', i.e. $d_{m\ell}^{\mathrm{U}} = 1, \forall m, \ell$, in (7). All the results are normalized as follows: for each m, α_m^{U} is set such that $|\tilde{s}_m^{\mathrm{U}}(t)|_{\max} = 1$ in (4b) and $x_m^{\mathrm{U}}(t)$ is divided by that α_m^{U} in (4c). As expected, the interference (MAI) floor $[x_m^{\mathrm{U}}(t)]$ decreases with increasing T_{b} due to decreasing overlap of MAI interferences of adjacent bits. The probability density function (PDF) of $x_m^{\mathrm{U}}(t)$ are found (third column in the figure) to closely follow the normal distribution PDF

$$\mathrm{PDF}(x_m^{\mathrm{U}}) = \frac{1}{\sqrt{2\pi\sigma^2}} \exp\left[-\frac{(x_m^{\mathrm{U}} - \mu_m)^2}{2\sigma_m^2} \right], \tag{10a}$$

where μ_m is the mean of x_m^{U}, which is 0 due to the symmetric-bipolar nature of MAI, and σ_m^2 is the variance,

$$\sigma_m^2 = \frac{1}{T_{\mathrm{b}}} \int_{T_{\mathrm{b}}} \left| x_m^{\mathrm{U}}(t) - \mu_m^{\mathrm{U}} \right|^2 dt = \frac{1}{T_{\mathrm{b}}} \int_{T_{\mathrm{b}}} \left| x_m^{\mathrm{U}}(t) \right|^2 dt, \tag{10b}$$

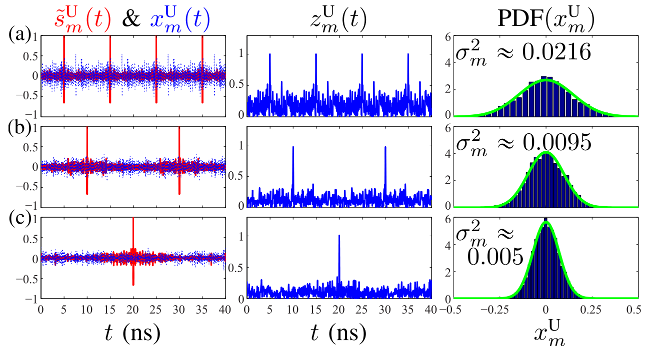

FIGURE 2. Uplink simulation results in the worst-case interference scenario, where $d_{m\ell}^{\mathrm{U}} = 1, \forall m, \ell$, in (7) for $M = 5$ TR-DCMA with $\Delta f = 10$ GHz, $\Delta\tau = 10$ ns, coding $\mathbf{C} = \{3, -3, 5, -5, 7\}$ and identical energy $\alpha_m^{\mathrm{U}} =$ const. in (3). All the results are normalized as follows: for each m, α_m^{U} is set such that $|\tilde{s}_m^{\mathrm{U}}(t)|_{\max} = 1$ in (4b) and $x_m^{\mathrm{U}}(t)$ is divided by that α_m^{U} in (4c). First column: desired signal, $\tilde{s}_m^{\mathrm{U}}(t)$ (red-solid curve), and MAI, $x_m^{\mathrm{U}}(t)$ (blue-dotted curve), computed using (4b) and (4c), respectively. Second column: total encoded signal, $z_m^{\mathrm{U}}(t)$, computed using (4a). Third column: probability density function (PDF) of the MAI values, obtained by counting the occurrences of the sample values (blue stripes) and compared against the normal distribution PDF (green curve) [Eq. (10a)] with mean $\mu_m = 0, \forall m$, and variance σ_m^2 in (10b). (a) $T_{\mathrm{b}} = \Delta\tau$, (b) $T_{\mathrm{b}} = 2\Delta\tau$, and (c) $T_{\mathrm{b}} = 4\Delta\tau$.

which is equivalent to the MAI average power over one bit. In a realistic scenario, where bits '1' and '0' alternate in the wireless channel, the interference would naturally be less, leading to smaller σ_m^2 values. In the forthcoming results, the same worst-case scenario has been assumed for the PDF, and practical results would then be better than what will be shown.

C. STATISTICAL AND ANALYTICAL SIR

The SIR may be statistically found by taking the ratio of $|\tilde{s}_m^{\mathrm{U}}(t)|_{\max}$ to the MAI variance given by (10b), using the normalization indicated in the caption of Fig. 2, which yields

$$\mathrm{SIR}_m^{\mathrm{U}\prime} = \frac{1}{\sigma_m^2}. \tag{11}$$

This quantity can also be obtained analytically as [12]

$$\mathrm{SIR}_m^{\mathrm{U}} = \frac{2\Delta f T_{\mathrm{b}}}{\overline{\alpha_m^2}(M-1)}, \tag{12a}$$

where

$$\overline{\alpha_m^2} = \frac{1}{M-1} \sum_{\substack{k=1 \\ k \neq m}}^{M} \left(\frac{\alpha_k^{\mathrm{U}}}{\alpha_m^{\mathrm{U}}} \right)^2 \tag{12b}$$

is the mean of the normalized MAI energies.[2]

Figure 3 compares the analytical [Eq. (12)] and statistical [Eq. (11)] SIRs. Good agreement is observed, with deviation smaller than 2 dB. Therefore, we will directly use (12) to avoid statistical testing over many bits in the remainder of the paper.

The downlink MAI also follows normal distribution, and the corresponding $\mathrm{SIR}_{n(m)}^{\mathrm{D}}$ is also approximated by (12) with α_k^{U} and α_m^{U} replaced by $\alpha_{n(k)}^{\mathrm{D}}$ and $\alpha_{n(m)}^{\mathrm{D}}$.

[2] In (12b), $k = m$ is excluded from the sum as it corresponds to the signal.

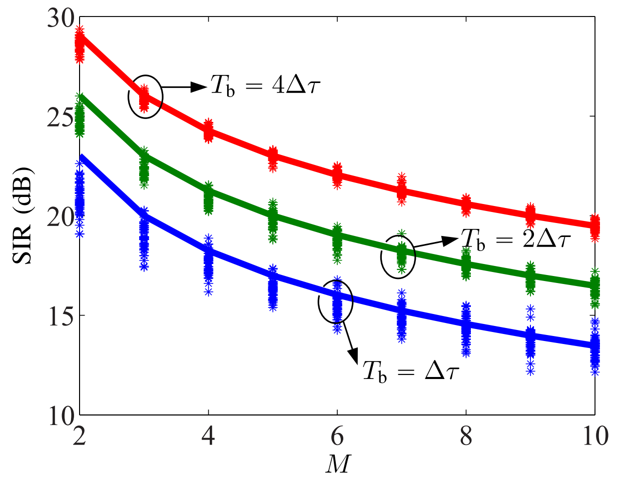

FIGURE 3. SIR versus the number of transmitters (M) with $\Delta f = 10$ GHz, $\Delta\tau = 10$ ns, coding $\mathbf{C} = \{3, -3, 5, -5, \ldots\}$, identical energy ($\alpha_m^{\mathrm{U}} =$ const. $\forall\, m$) in (3), and different T_{b}. Solid curves: Eq. (12), '*' markers: Eq. (11) with (10b) and (4c) for 500 bits.

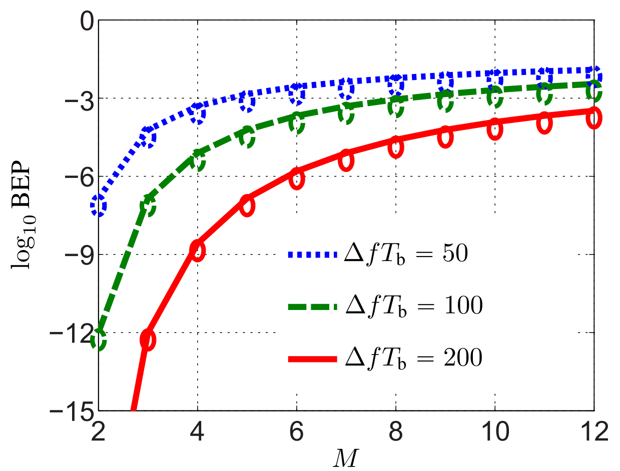

FIGURE 4. BEP versus the number of simultaneous communication links (M) in the TR-DCMA system in Fig. 1 for APs with identical energy ($\alpha_m^{\mathrm{U}} = \alpha_{n(m)}^{\mathrm{D}} =$ const. $\forall\, m$), computed using (14) (curves), and compared against the BEP of the corresponding DCMA system without time-reversal routing [12] (circles), for different $\Delta f T_{\mathrm{b}}$ values.

D. OVERALL BEP PERFORMANCE

The BEP for MAI with normal distribution is [12]

$$\mathrm{BEP}_m^{\mathrm{U}} = \frac{1}{\sqrt{2\pi}} \int_{\sqrt{\mathrm{SIR}_m^{\mathrm{U}}/2}}^{+\infty} \exp\left(-\frac{x^2}{2}\right) dx, \tag{13}$$

where $\mathrm{SIR}_m^{\mathrm{U}}$ is given by (12). The downlink $\mathrm{BEP}_{n(m)}^{\mathrm{D}}$ is found by replacing $\mathrm{SIR}_m^{\mathrm{U}}$ in (13) with $\mathrm{SIR}_{n(m)}^{\mathrm{D}}$.

Communication is overall successful if both the uplink and downlink transmissions are successful, corresponding to the overall BEP

$$\begin{aligned}\mathrm{BEP}_m &= 1 - \left(1 - \mathrm{BEP}_m^{\mathrm{U}}\right)\left(1 - \mathrm{BEP}_{n(m)}^{\mathrm{D}}\right) \\ &= \mathrm{BEP}_m^{\mathrm{U}} + \mathrm{BEP}_{n(m)}^{\mathrm{D}} - \mathrm{BEP}_m^{\mathrm{U}}\mathrm{BEP}_{n(m)}^{\mathrm{D}} \\ &\approx \mathrm{BEP}_m^{\mathrm{U}} + \mathrm{BEP}_{n(m)}^{\mathrm{D}}. \end{aligned} \tag{14}$$

Figure 4 plots the BEP (same for all m's) of the TR-DCMA system for APs with identical energy, and compared against that of the corresponding DCMA system without time-reversal routing. Due to the two-step (uplink and downlink) transmission phases, the BEP is approximately doubled, or degraded by an order of $\log_{10} 2 \approx 0.3$. This graph shows that the BEP is not affected by the dynamic TR routing. The convergence of the 3 curves as M increases is due to accumulation of interference, or SIR degradation towards 0. The convergence value can be found by setting SIR $= 0$ in (13), which results in $\mathrm{BEP}_m^{\mathrm{U}} = 0.5 = \mathrm{BEP}_{(m)}^{\mathrm{D}}$, then inserting this result into (14), which leads to 0.75 (-0.125 dB).

V. CONCLUSION

A TR-DCMA routing system has been presented and characterized in terms of MAI statistical distributions, SIR, and BEP. The system may find its applications in dynamic wireless communications requiring low-complexity transceivers and negligible latency.

REFERENCES

[1] C. Caloz, S. Gupta, Q. Zhang, and B. Nikfal, "Analog signal processing: A possible alternative or complement to dominantly digital radio schemes," *IEEE Microw. Mag.*, vol. 14, no. 6, pp. 87–103, Sep. 2013.

[2] S. Gupta, Q. Zhang, L. Zou, L. Jiang, and C. Caloz, "Generalized coupled-line all-pass phasers," *IEEE Trans. Microw. Theory Techn.*, vol. 63, no. 3, pp. 1007–1018, Mar. 2015.

[3] M. A. G. Laso *et al.*, "Real-time spectrum analysis in microstrip technology," *IEEE Trans. Microw. Theory Techn.*, vol. 51, no. 3, pp. 705–717, Mar. 2003.

[4] B. Nikfal, D. Badiere, M. Repeta, B. Deforge, S. Gupta, and C. Caloz, "Distortion-less real-time spectrum sniffing based on a stepped group-delay phaser," *IEEE Microw. Wireless Compon. Lett.*, vol. 22, no. 11, pp. 601–603, Nov. 2012.

[5] J. D. Schwartz, J. Azana, and D. V. Plant, "A fully electronic system for the time magnification of ultra-wideband signals," *IEEE Trans. Microw. Theory Techn.*, vol. 55, no. 2, pp. 327–334, Feb. 2007.

[6] B. Xiang, A. Kopa, Z. Fu, and A. B. Apsel, "Theoretical analysis and practical considerations for the integrated time-stretching system using dispersive delay line (DDL)," *IEEE Trans. Microw. Theory Techn.*, vol. 60, no. 11, pp. 3449–3457, Nov. 2012.

[7] B. Nikfal, S. Gupta, and C. Caloz, "Increased group-delay slope loop system for enhanced-resolution analog signal processing," *IEEE Trans. Microw. Theory Techn.*, vol. 59, no. 6, pp. 1622–1628, Jun. 2011.

[8] J. D. Schwartz, J. Azaña, and D. V. Plant, "An electronic temporal imaging system for compression and reversal of arbitrary UWB waveforms," in *Proc. IEEE Radio Wireless Symp.*, Orlando, FL, USA, Jan. 2008, pp. 487–490.

[9] S. Gupta, B. Nikfal, and C. Caloz, "Chipless RFID system based on group delay engineered dispersive delay structures," *IEEE Antennas Wireless Propag. Lett.*, vol. 10, pp. 1366–1368, Oct. 2011.

[10] B. Nikfal, Q. Zhang, and C. Caloz, "Enhanced-SNR impulse radio transceiver based on phasers," *IEEE Microw. Wireless Compon. Lett.*, vol. 24, no. 11, pp. 778–780, Nov. 2014.

[11] S. Gupta, L. Zou, M. A. Salem, and C. Caloz, "Bit-error-rate (BER) performance in dispersion code multiple access (DCMA)," in *Proc. IEEE Int. Symp. Antennas Propag.*, Jul. 2015, pp. 1015–1016.

[12] L. Zou, S. Gupta, and C. Caloz, "Real-time dispersion code multiple access for high-speed wireless communications," *IEEE Trans. Wireless Commun.*, vol. 17, no. 1, pp. 266–281, Jan. 2018. [Online]. Available: http://ieeexplore.ieee.org/document/8086172/

[13] A. Osseiran, J. F. Monserrat, and P. Marsch, *5G Mobile and Wireless Communications Technology*. Cambridge, U.K.: Cambridge Univ. Press, 2016.

[14] L. Zou, S. Gupta, and C. Caloz, "Loss-gain equalized reconfigurable C-section analog signal processor," *IEEE Trans. Microw. Theory Techn.*, vol. 65, no. 2, pp. 555–564, Feb. 2017.

[15] M. Fink, "Time reversal of ultrasonic fields. I. Basic principles," *IEEE Trans. Ultrason., Ferroelect., Freq. Control*, vol. 39, no. 5, pp. 555–566, Sep. 1992.

[16] G. Lerosey, J. de Rosny, A. Tourin, A. Derode, G. Montaldo, and M. Fink, "Time reversal of electromagnetic waves," *Phys. Rev. Lett.*, vol. 92, no. 19, p. 193904, May 2004.

[17] A. F. Molisch, *Wireless Communications*, 2nd ed. Hoboken, NJ, USA: Wiley, 2011.

[18] J. Zhang and J. Yao, "Photonic-assisted microwave temporal convolution," *J. Lightw. Technol.*, vol. 34, no. 20, pp. 4652–4657, Oct. 15, 2016.

[19] E. Dahlman, S. Parkvall, and J. Sköld, *4G: LTE/LTE-Advanced for Mobile Broadband*, 2nd ed. Oxford, U.K.: Elsevier, 2014.

[20] J. R. Foerster, M. Pendergrass, and A. F. Molisch, "A channel model for ultrawideband indoor communication," Mitsubishi Electr. Res. Lab., Cambridge, MA, USA, Tech. Rep. TR-2003-73, Nov. 2003.

LIANFENG ZOU received the B.Eng. degree in electromagnetic field and microwave technology from the University of Electronic Science and Technology of China, Chengdu, China, in 2004, the M.E. degree in electronic science and technology from the Graduate University of Chinese Academy of Sciences, Beijing, China, in 2007, and the Ph.D. degree from the École Polytechnique de Montréal, Montréal, QC, Canada, in 2017. From 2007 to 2012, he was as an RF Engineer with the China Electronics Group Corporation. His research interests include dispersion engineered structures and their applications in the real-time analog signal processing for future millimeter-wave and terahertz radio systems.

CHRISTOPHE CALOZ (F'10) received the Diplôme d'Ingénieur degree en électricité and Ph.D. degree from the École Polytechnique Fédérale de Lausanne, Switzerland, in 1995 and 2000, respectively. From 2001 to 2004, he was a Post-Doctoral Research Fellow with the Microwave Electronics Laboratory, University of California at Los Angeles (UCLA). In 2004, he joined the École Polytechnique of Montréal, where he is currently a Full Professor, holds the Canada Research Chair Tier-I, and is the Head of the Electromagnetics Research Group. In 2009, he co-founded the company ScisWave (now Tembo Networks). He has authored or co-authored over 700 technical conference, letter, and journal papers, and 13 books and book chapters, and holds several patents. His research interests include all fields of theoretical, computational, and technological electromagnetics, with a strong emphasis on emergent and multidisciplinary topics, including particularly metamaterials, nanoelectromagnetics, exotic antenna systems, and real-time radio. His research has generated about 20 000 citations, and he has been the Thomson Reuters Highly Cited Researcher. He was a member of the IEEE Microwave Theory and Techniques Society (MTT-S), Technical Committees MTT-15 (Microwave Field Theory), and MTT-25 (RF Nanotechnology), a Speaker of the MTT-15 Speaker Bureau, the Chair of the Commission D (Electronics and Photonics) of the Canadian Union de Radio Science Internationale and an MTT-S representative at the IEEE Nanotechnology Council. He was the recipient of several awards, including the UCLA Chancellor's Award for Post-doctoral Research in 2004, the MTT-S Outstanding Young Engineer Award in 2007, the E. W. R. Steacie Memorial Fellowship in 2013, the Prix Urgel-Archambault in 2013, the Killam Fellowship in 2016, and many Best Paper Awards with his students at international conferences. He has been an IEEE Distinguished Lecturer for the Antennas and Propagation Society (AP-S) since 2014 and a Fellow of the Canadian Academy of Engineering since 2016. In 2014, he was elected as a member of the Administrative Committee of AP-S. He was a Distinguished Adjunct Professor with King Abdulaziz University, Saudi Arabia, from 2014 to 2015. He was an Associate Editor of the IEEE TRANSACTIONS ON ANTENNAS AND PROPAGATION from 2015 to 2017.